# Vehicle-Vehicle Energy Interaction Converter of Electric Vehicles: A Disturbance Observer Based Sliding Mode Control Algorithm.

Wang, Rui; Sun, Qiuye; Sun, Chenghao; Zhang, Huaguang; Gui, Yonghao; Peng, Wang

*Published in:*
I E E E Transactions on Vehicular Technology

*DOI (link to publication from Publisher):*
10.1109/TVT.2021.3105433

*Publication date:*
2021

*Document Version*
Accepted author manuscript, peer reviewed version

# Vehicle-Vehicle Energy Interaction Converter of Electric Vehicles: A Disturbance Observer Based Sliding Mode Control Algorithm

Rui Wang, *Student Member, IEEE*, Qiuye Sun, *Senior Member, IEEE*, Chenghao Sun, *Student Member, IEEE*, Huaguang Zhang, *Fellow, IEEE*, Yonghao Gui, *Senior Member, IEEE*, Peng Wang, *Fellow, IEEE*

***Abstract*—The electric vehicle technology is one of the most promising candidates to reduce fuel consumption and $CO_2$ emission. Although electric vehicles have been widely promoted by governments around the world, their development is seriously hampered due to charger unavailability and range anxiety. Based on this, this paper designs an energy interaction converter between two electric vehicles, which is controlled through disturbance observer based sliding mode control algorithm. For this converter, three main demands should be satisfied, i.e., high power density, weak source and constant power load. Therein, weak source whose minimum short circuit ratio (SCR) belongs to [2,3], is always called weak grid. Firstly, the equivalent impedance switching process is introduced to eliminate the impact of weak source. Meanwhile, the equivalent six channel interleaved floating dual boost converter is chosen to satisfy the high power density demand, whose generalized state-space function is further built to provide an indispensable preprocessing for following controller design. Moreover, in order to solve the problem regarding low frequency/sub-synchronous oscillation caused through constant power load feature regarding the energy consumption vehicle and weak source feature regarding the energy supply vehicle, a disturbance observer based sliding mode control algorithm is proposed through using generalized state-space function to provide standard DC power with both constant voltage and power. Furthermore, the proportional-resonant controller is proposed to solve the current sharing problem among six parallel channels, which reduces the heat loss and improves the service life of the device. Finally, simulation and experimental results verify the high performance of the proposed control algorithm.**

***Index Terms*—electric vehicle, energy interaction converter, impedance switching, sliding mode control.**

## I. Introduction

THE Paris Conference in 2015 has provided one guide to restrict climate variation "well below 2 degrees C" [1], which has triggered the studies for clean alternative fuels for transportation. To this end, the electric vehicle technology has become one of the most promising candidates at present [2]-[3]. Although the electric vehicle has been widely promoted by governments around the world, three main problems still hinder the development of electric vehicles, i.e., charger unavailability, range anxiety and high prices. Therein, the high price has been alleviated through subsidized charging programmes and tax breaks [4]-[5]. However, it is urgent for scholars to deal with charger unavailability and range anxiety. Based on this, this paper designs an energy interaction converter between two electric vehicles, which is controlled through disturbance observer based sliding mode control algorithm.

Once battery mileage problem such as lack of electricity in the middle of the way occurs in electric vehicles, vehicle owners could only rescue and wait for rescue through mobile communication devices, which reduces the buying enthusiasm regarding electric vehicles. In order to solve this problem, it is advisable that electric vehicles charge each other through portable energy interaction converter. Therein, the energy supply vehicle can be regarded as one weak source, and the energy consumption vehicle always adopts constant power charge mode, which can be regarded as one constant power load [6]. However, the instability caused through weak source and constant power load has been widely reported such as low-frequency oscillation and sub-synchronous oscillation [7]-[8]. To sum up, three major challenges such as high power density, weak source and constant power load should be solved.

For constant power loads, plenty of scholars proposed numerous approaches, which could be divided into linear control strategy and nonlinear control strategy [7], [9]-[20]. From the viewpoint of the linear control strategy, the passive damping control technology was proposed to achieve the system stability operation through adding passive components such as capacitors/resistors [9]-[10]. However, the additional physical components were bound to increase the cost and consumption of the system. Based on this, the active damping technology was proposed through virtual impedance injection, which could improve the stability margin and response speed of the system at the same time [11]-[12]. However, the foresaid linear control technologies are based on the linear model under small signal, which is difficult for scholars to adopt in the vehicle-vehicle energy interaction converter of electric vehicles [13].

Different from the linear control strategy, the nonlinear control technology could realize fast energy interaction control among main grid and loads [7]. Firstly, feedback linearization

This work is supported by National Key Research and Development Program of China (2018YFA0702200), National Natural Science Foundation of China (62073065). (*Corresponding authors: Qiuye Sun*)

Rui Wang, Qiuye Sun, Chenghao Sun and Huaguang Zhang are with the Northeastern University, Liaoning, 110819, China. (E-mail: wangrui@ise.neu.edu.cn; sunqiuye@ise.neu.edu.cn; sunchenghaoneu@163.com; hgzhang@ieee.org).

Gui Yonghao was with the Automation & Control Section at the Dept. Electronic Systems, Aalborg University, 9220 Aalborg, Denmark. (e-mail: yg@es.aau.dk.)

Peng Wang is with the School of Electrical and Electronic Engineering, Nanyang Technological University, 639798, Singapore. (E-mail: epwang@ntu.edu.sg).

technique was proposed to eliminate the negative impedance characteristic and nonlinear term caused through constant power loads [14]-[15]. However, compared with other nonlinear control strategies, this technique had obvious defects such as slow dynamic response and unclear disturbance mechanism. To that end, the conventional input-output linearization strategy was proposed to realize the safe and stable operation of constant power loads, whose essence was to transform non-minimum phase system into minimum phase system [16]. Nevertheless, it was difficult to determine the accurate equivalent impedance of the electric system. The real-time nonlinear model predictive controller was proposed for direct yaw moment control of distributed drive electric vehicles, which achieved real-time optimization [17]-[18]. However, this method focused more on Magic Formula (MF) tire model. Furthermore, the model predictive control based on high-order sliding mode observer was proposed to realize the stable operation of boost converter with constant power loads. High order sliding mode observer could eliminate the impact of negative impedance and circuit parameter uncertainty, which was, however, required very high computing power [19]. Clearly, the processor in the convenient energy interaction converter was difficult to satisfy the relevant requirements. For the conventional boost converter with unknown line parameters and constant power loads, the disturbance observer based on back-stepping was proposed to achieve accurate tracking and stable operation under disturbance in the literature [20]. Nevertheless, it needed to make strict assumptions about the unknown types of line parameters, which restricted its application in practical systems. Recently, the sliding mode control approach was proposed to ensure the stable operation of step-up transformer under constant power loads, which was regarded as an active stabilization control [21]-[22]. Firstly, the fixed frequency sliding mode control strategy with constant power load was proposed to ensure the stable operation of the system [21]. However, it required additional current sensors such that the hardware cost and equivalent output impedance were increased. Furthermore, the robust sliding mode control strategy was proposed for the conventional boost converter in the literature [22]. Therein, it was very sensitive to the DC source voltage and was necessary to assume that the supply side voltage of the system was constant, which was difficult for practical electric vehicles. Thus, it is urgent for scholars to propose a suitable control strategy for the energy interaction converter of electric vehicles.

In order to achieve the energy interaction between two electric vehicles, this paper designs an energy interaction converter controlled through disturbance observer based sliding mode control algorithm. The main advantages of the proposed method are shown as follows:

1) The energy interaction converter with weak source and constant power load is switched to the parallel six channel interleaved floating dual boost converter with partial unknown circuit parameters, which is further built as one state-space function with unknown parameters. With these effects, the demands regarding high power density and weak source can be satisfied;

2) Based on the foresaid state-space function, an energy interaction converter controlled through disturbance observer based sliding mode control algorithm is designed in this paper. Under this approach, the demand regarding constant power load can be satisfied. Furthermore, the proportional-resonant controller is proposed to solve the current sharing problem caused through proposed six parallel channels, which reduces the heat loss and improves the service life of the energy interaction converter.

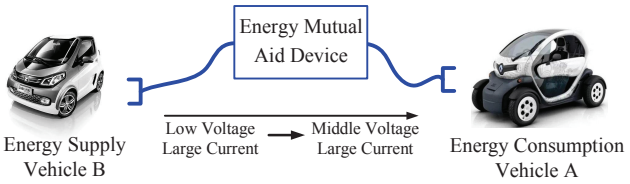


Fig. 1: Portable electric vehicle energy interaction converter.

The rest of the paper is shown as follows. In Section II, the state-space function with partial unknown parameters regarding energy interaction converter consisting of weak source and constant power load is built. Furthermore, an energy interaction converter controlled through disturbance observer based sliding mode control algorithm is designed in Section III. Moreover, the proportional-resonant controller is proposed to achieve accurate current sharing in Section IV. Meanwhile, the simulation and experiment results are provided to validate the performance of the proposed approach in Section V and Section VI. Eventually, this paper is concluded in Section VII.

## II. Modified six channel interleaved floating dual boost converter and its state-space function

If the battery energy of the electric vehicle is insufficient and cannot be charged nearby through the charging station, the electric vehicle owner can use the portable electric vehicle energy interaction converter shown in Fig. 1, to obtain power energy from the electric vehicle whose battery is plentiful. Among them, the electric vehicle with insufficient electric energy can be defined as the energy consumption vehicle A, and the electric vehicle with abundant electric energy is defined as the energy supply vehicle B. Since each electric vehicle has four to six batteries and the output voltage of each battery is 15V, the practical output voltage regarding the energy supply vehicle B is approximately $60V$. Meanwhile, the input voltage regarding the energy consumption vehicle A is $250V$ [6]. In order to satisfy the fast charge between two electric vehicles, the transmission power is expected to be more than $20kW$. Thus, the high power density should be achieved.

Since the supply power source regarding electric vehicles belongs to the weak source, the practical source for the energy interaction converter can be equivalent to the Thevenin equivalent circuit, which is shown in Fig. 2 [23]. Therein, equivalent inductance can be represented as $L_g = 1/SCR[p.u.]$ [24], $SCR$ represents the minimum short circuit ratio, which is often used to characterize the strength of the grid. According to IEEE 1204-1997 standard, the system belongs to weak gird if $SCR \in [2, 3]$ [25].

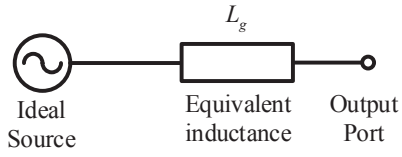


Fig. 2: Thevenin equivalent of weak source.

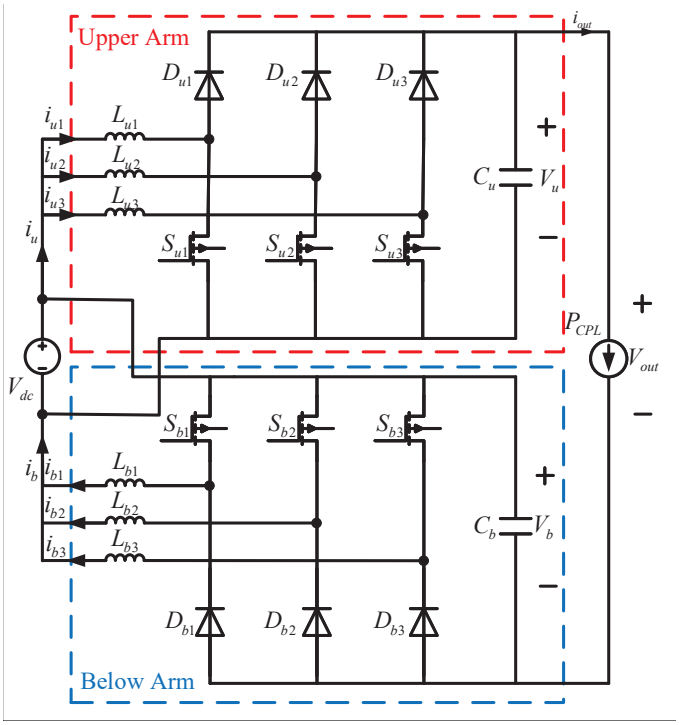


Fig. 3: Hardware topology of the energy interaction converter

Due to the high power density demand, the energy interaction converter adopts the six channel interleaved floating dual boost converter in this paper, which is shown in Fig. 3, where the DC source $V_{dc}$ is the weak source of the energy supply vehicle B and the energy consumption vehicle A is regarded as one constant power load $P_{CPL}$. $L_{u1}$ to $L_{u3}$ represent inductances of the three channels in the upper bridge arm, respectively. $L_{b1}$ to $L_{b3}$ represent inductances of the three channels in the below bridge arm, respectively. Noting that $L_{u1}$ to $L_{u3}$ and $L_{b1}$ to $L_{b3}$ belong to the inner structure regarding the converter. $i_{u1}$ to $i_{u3}$ represent currents of the three channels in the upper bridge arm, respectively. $i_{b1}$ to $i_{b3}$ represent currents of the three channels in the below bridge arm, respectively. $V_u$, $i_u$ and $C_u$ represent the output voltage, current and capacitor of the upper bridge arm regarding the energy interaction converter, respectively. $V_b$, $i_b$ and $C_b$ represent the output voltage, current and capacitor of the below bridge arm regarding the energy interaction converter, respectively. Noting that $i_{out} = P_{CPL}/V_{out}$.

In order to eliminate the impact of the equivalent inductance of the weak source ($L_g$) and facilitate the controller design, the equivalent impedance switching process can be proposed in this section, which is shown in Fig. 4. Due to the existence of current sharing controller, the current flowing through each path is the same, i.e., $i_1 = i_2 = ... = i_n$. According

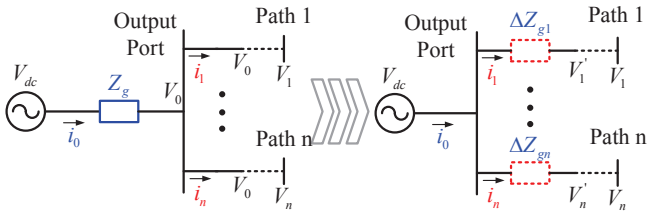


Fig. 4: Equivalent impedance switching process

to our previous literature [26], the equivalent inductance is transformed into the same inductance in each path, e.g., $\Delta L_{g1} = ... = \Delta L_{gn}$. Since the model of each battery regarding electric vehicle is unknown, it is difficult to acquire the equivalent inductance in advance, that is, $\Delta L_{g1} = ... = \Delta L_{gn}$ is unknown. Thus, the weak source demand should be achieved through embedding equivalent inductance to state-space function of the energy interaction converter.

To sum up, according to Kirchhoff voltage/current law and model average modeling technology, the average model of the upper bridge arm is shown as follows :

$$(L_{ui} + \Delta L_{gui}) \frac{di_{ui}}{dt} = V_{dc} - (1 - u_{ui}) V_u \tag{1}$$

$$C_u \frac{dV_u}{dt} = \sum_{i=1}^{3} i_u (1 - u_{ui}) - i_{out} \tag{2}$$

where $u_{ui}$ represents the duty cycle of the $i^{th}$ channel of the upper arm of the energy interaction converter, and $\Delta L_{gui}$ represents the unknown equivalent power inductance of the $i$-channel of the upper arm. Since the energy interaction converter is symmetrical, $L_{u1} = L_{u2} = L_{u3}$. At the same time, due to the existence of averaging controller, $i_{u1} = i_{u2} = i_{u3}$. Therefore, the generalized reduced order average model of the upper arm is as follows:

$$(L_u + \Delta L_{gu}) \frac{di_u}{dt} = V_{dc} - (1 - u_u) V_u \tag{3}$$

$$(C_u + \Delta C_u) \frac{dV_u}{dt} = i_u (1 - u_u) - i_{out} \tag{4}$$

where $L_u = \frac{1}{3} L_{ui}$ represents the primary inductance of the upper arm equivalent boost converter; $\Delta L_{gu} = \frac{1}{3} \Delta L_{gui}$ represents equivalent weak source inductance of upper bridge arm; $\Delta C_u$ represents capacitance uncertainty caused by parasitic capacitance of upper bridge arm; $u_u$ represents equivalent duty cycle of upper arm. i.e., $u_u = u_{ui}$. Noting that the state space model in this paper is still one state-space function with partial unknown parameters. In order to solve these unknown parameters, one disturbance observer is designed in Section III. Similarly, the generalized reduced order average model of the lower arm is shown as follows:

$$(L_b + \Delta L_{gb}) \frac{di_b}{dt} = V_{dc} - (1 - u_b) V_b \tag{5}$$

$$(C_b + \Delta C_b) \frac{dV_b}{dt} = i_b (1 - u_b) - i_{out} \tag{6}$$

where $L_b = \frac{1}{3}L_{bi}$ represents the primary inductance of the lower arm equivalent boost converter; $\Delta L_{gb} = \frac{1}{3}\Delta L_{gbi}$ represents equivalent weak source inductance of lower bridge arm; $\Delta C_b$ represents capacitance uncertainty caused by parasitic capacitance of lower bridge arm; $u_b$ represents equivalent duty cycle of lower arm. i.e., $u_b = u_{bi}$. There is no doubt that $L_u = L_b = L$. According to Kirchhoff voltage law, it can be seen that:

$$V_{out} = V_u + V_b - V_{dc} \tag{7}$$

Therefore, the control objective of this paper is to accurately control the output voltage of the upper/lower bridge arms, i.e. $V_u$ and $V_b$, to ensure that the output voltage of the energy interaction converter can reach the rated input voltage of distributed generator. To this end, the output voltage of the upper/lower arm should be controlled to $V_u = V_b = V^*_{ref}$ where $V^*_{ref} = (V_{ref} + V_{dc})/2$. Therein, $V_{ref}$ represents the whole output voltage of the portable electric vehicle energy interaction converter, $V^*_{ref}$ represents the output voltage of the upper arm or below arm regarding the portable electric vehicle energy interaction converter. For this energy interaction converter, the input variables are current ($i_u$ and $i_b$) and voltage ($V_u$, $V_b$ and $V_{dc}$). Meanwhile, the output variables are switching signals ($u_{ph1}$ to $u_{ph6}$). In order to satisfy the demands regarding weak source and constant power load, three controllers should be designed. Therein, the disturbance observer should be designed to solve the partial unknown parameters, and sliding mode controller should be designed to make the output voltage of the upper/lower arm be controlled to $V_u = V_b = V^*_{ref}$. Finally, the proportional-resonant controller is proposed to solve the current sharing problem caused through proposed six parallel channels.

## III. Disturbance observer based sliding mode control algorithm

In order to satisfy the constant power load demand, the disturbance observer based sliding mode control algorithm is proposed in this section, which should provide stable output voltage of the modified six channel interleaved floating dual boost converter under variation of source and load. In order to considering the constant power load in terms of linear approach, the generalized average model (3)-(6) proposed in the foresaid section should be transformed into one linear standard system to design sliding mode control based on disturbance observer. Firstly, a series of state variables are defined to describe the energy interaction converter

$$x_1 = 0.5Li_u^2 + 0.5C_uV_u^2 \tag{8}$$
$$x_2 = V_{dc}i_u \tag{9}$$
$$x_3 = 0.5Li_b^2 + 0.5C_bV_b^2 \tag{10}$$
$$x_4 = V_{dc}i_b \tag{11}$$

where $x_1$ and $x_3$ represent the energy of the upper/lower arm of the energy interaction converter, and $x_2$ and $x_3$ represent the output power of the upper/lower arm of the energy interaction converter. Then, the derivative calculation is carried out and the following results are obtained

$$\dot{x}_1 = Li_u\dot{i}_u + C_uV_u\dot{V}_u \tag{12}$$
$$\dot{x}_2 = V_{dc}\dot{i}_u \tag{13}$$
$$\dot{x}_3 = Li_b\dot{i}_b + C_bV_b\dot{V}_b \tag{14}$$
$$\dot{x}_4 = V_{dc}\dot{i}_b \tag{15}$$

By substituting equation (3)-(6) into equation (12)-(15):

$$d_1 = -V_ui_{out} - \frac{\Delta L_{gu}}{L + \Delta L_{gu}}\left[V_{dc} - (1-u_u)V_u\right] - \frac{\Delta C_uV_u}{C_u + \Delta C_u}\left[(1-u_u)i_u - i_{out}\right] \tag{16}$$
$$d_2 = \frac{-V_{dc}\Delta L_{gu}}{L(L + \Delta L_{gu})}\left[V_{dc} - (1-u_u)V_u\right] \tag{17}$$
$$d_3 = -V_bi_{out} - \frac{\Delta L_{gb}}{L_b + \Delta L_{gb}}\left[V_{dc} - (1-u_b)V_b\right] - \frac{\Delta C_bV_b}{C_b + \Delta C_b}\left[(1-u_b)i_b - i_{out}\right] \tag{18}$$
$$d_4 = \frac{-V_{dc}\Delta L_{gb}}{L(L + \Delta L_{gb})}\left[V_{dc} - (1-u_b)V_b\right] \tag{19}$$
$$h_1 = \frac{V_{dc}^2}{L} - \frac{(1-u_u)V_{dc}V_u}{L} \tag{20}$$
$$h_2 = \frac{V_{dc}^2}{L} - \frac{(1-u_b)V_{dc}V_b}{L} \tag{21}$$

Therefore, the equation of state (12)-(15) can be rewritten:

$$\dot{x}_1 = x_2 + d_1 \tag{22}$$
$$\dot{x}_2 = h_1 + d_2 \tag{23}$$
$$\dot{x}_3 = x_3 + d_3 \tag{24}$$
$$\dot{x}_4 = h_2 + d_4 \tag{25}$$

where $h_1$ and $h_2$ represent the virtual control quantities of the upper and lower arms respectively. It should be noted that equations (22)-(25) are differential homeomorphic maps of the primitive system (3)-(6) [27]. Based on the operation mechanism of the energy interaction converter, the following components can be ignored, i.e., $[V_{dc} - (1-u_u)V_u]$, $[(1-u_u)i_u - i_{out}]$, $[V_{dc} - (1-u_b)V_b]$ and $[(1-u_b)i_b - i_{out}]$. Therefore, disturbances $d_1$ and $d_2$ can be simplified as follows:

$$d_1 = -V_ui_{out} \tag{26}$$
$$d_3 = -V_bi_{out} \tag{27}$$

Using equations (16)-(21), the actual control variables of the controller can be obtained as follows:

$$u_u = 1 - \frac{V_{dc}^2 - Lh_1}{V_{dc}V_u} \tag{28}$$
$$u_b = 1 - \frac{V_{dc}^2 - Lh_2}{V_{dc}V_b} \tag{29}$$

After the coordinate transformation of the differential homeomorphism mapping, the objectives of the controller are transformed from $V_{out}$ tracking $V_{ref}$ to state variables $x_1$ and $x_3$, which converge gradually to their rated values, i.e. $x_{1ref}$

and $x_{3ref}$, which is shown as follows:

$$\begin{aligned} x_{1ref} &= 0.5Li_{uref}^2 + 0.5C_uV_{uref}^2 && (30)\\ x_{2ref} &= V_{dc}i_{uref} && (31)\\ x_{3ref} &= 0.5Li_{bref}^2 + 0.5C_bV_{bref}^2 && (32)\\ x_{4ref} &= V_{dc}i_{bref} && (33) \end{aligned}$$

where $V_{uref} = V_{bref} = V_{ref}^*$. $i_{uref}$ and $i_{bref}$ represent the input current reference value of the upper/lower bridge arm, respectively. Taking into account the conservation of input/output power, $i_{uref}$ and $i_{bref}$ can be expressed:

$$i_{uref} = i_{bref} = \frac{V_{ref}^* i_{out}}{V_{dc}} \tag{34}$$

Since the disturbances $d_1$ to $d_4$ are composed of uncertainties caused by output current and weak source/parasitic capacitance, they and their derivatives have extremum, i.e., $d_{i\max} = \sup_{t>0}|d_i(t)|$ and $\tilde{d}_{i\max} = \sup_{t>0}\left|\dot{d}_i(t)\right|$. At the same time, the final value of its derivative tends to zero in steady state. Based on equations (26) - (27), the instantaneous value of the output current of the energy interaction converter can be obtained by disturbances $d_1$ and $d_3$. Therefore, rating $x_{1ref}$ to $x_{4ref}$ of the state variable can be accurately obtained through observing $d_1$ and $d_3$. Based on this, a disturbance observer is designed in this paper

$$\begin{cases} \hat{d}_1 = H_{d1}x_1 + \alpha_1 \\ \dot{\alpha}_1 = -H_{d1}\left(x_2 + \hat{d}_1\right) \end{cases} \tag{35}$$

$$\begin{cases} \hat{d}_2 = H_{d2}x_2 + \alpha_2 \\ \dot{\alpha}_2 = -H_{d2}\left(h_1 + \hat{d}_2\right) \end{cases} \tag{36}$$

$$\begin{cases} \hat{d}_3 = H_{d3}x_3 + \alpha_3 \\ \dot{\alpha}_3 = -H_{d3}\left(x_4 + \hat{d}_3\right) \end{cases} \tag{37}$$

$$\begin{cases} \hat{d}_4 = H_{d4}x_4 + \alpha_4 \\ \dot{\alpha}_4 = -H_{d4}\left(h_2 + \hat{d}_4\right) \end{cases} \tag{38}$$

where $\hat{d}_1$ to $\hat{d}_4$ represent the observed values of disturbance $d_1$ to $d_4$; $H_{d1}$ to $H_{d4}$ represent the positive observation gains; $\alpha_1$ to $\alpha_4$ represent the internal variables of the observer. Using equations (35)-(38), the observer error dynamic characteristics are as follows:

$$\begin{aligned} \dot{e}_{d1} &= -H_{d1}e_{d1} + \dot{d}_1 && (39)\\ \dot{e}_{d2} &= -H_{d2}e_{d2} + \dot{d}_2 && (40)\\ \dot{e}_{d3} &= -H_{d3}e_{d3} + \dot{d}_3 && (41)\\ \dot{e}_{d4} &= -H_{d4}e_{d4} + \dot{d}_4 && (42) \end{aligned}$$

where $e_{di} = d_i - \hat{d}_i$ represents observer error. The following energy functions are constructed

$$Q(e_{d1}, e_{d2}, e_{d3}, e_{d4}) = 0.5\sum_{i=1}^{4} e_{di}^2 \tag{43}$$

Therefore, the following inequality can be obtained

$$\begin{aligned} \dot{Q}(e_{di}) &= \sum_{i=1}^{4}\left(-H_{di}e_{di}^2 + e_{di}\dot{d}_i\right) \\ &\le \sum_{i=1}^{4}\left(-H_{di}|e_{di}|^2 + |e_{di}|\,\tilde{d}_{i\max}\right) \\ &= -\sum_{i=1}^{4}|e_{di}|\left(H_{di}|e_{di}| - \tilde{d}_{i\max}\right) && (44) \end{aligned}$$

Therefore, in a finite time, the estimation error is finite and the boundary is shown as follows:

$$|e_{di}| \le \sigma_d \tag{45}$$

where $\sigma_d = \max\left(\tilde{d}_{i\max}/H_{di}\right)$. Since unknown parameters are embedded into the state space model, the disturbance observer based sliding mode control algorithm should be proposed in this paper. Based on equations (26)-(27) and (30)-(34), the estimated reference values of the state variables are shown as follows:

$$\begin{aligned} \hat{x}_{1ref} &= 0.5L\frac{\hat{d}_1^2}{V_{dc}^2} + 0.5C_uV_{ref}^{*2} && (46)\\ \hat{x}_{2ref} &= -\hat{d}_1 && (47)\\ \hat{x}_{3ref} &= 0.5L\frac{\hat{d}_3^2}{V_{dc}^2} + 0.5C_bV_{ref}^{*2} && (48)\\ \hat{x}_{4ref} &= -\hat{d}_3 && (49) \end{aligned}$$

Furthermore, a sliding mode controller based on disturbance observer is proposed, and its sliding surface is shown as follows:

$$\begin{aligned} s_1 &= a_1e_{x1} + e_{x2} - \dot{\hat{x}}_{1ref} && (50)\\ s_2 &= a_2e_{x3} + e_{x4} - \dot{\hat{x}}_{3ref} && (51) \end{aligned}$$

Among them, $e_{xi} = x_i - x_{iref}$ is called the state deviation; $\dot{\hat{x}}_{1ref}$ and $\dot{\hat{x}}_{3ref}$ represent the derivatives of $\hat{x}_{1ref}$ and $\hat{x}_{3ref}$. In order to ensure that the sliding surfaces $s_1$ and $s_2$ converge to zero, the following controllers are designed:

$$\begin{aligned} h_1 &= -a_1\left(e_{x2} - \dot{\hat{x}}_{1ref}\right) + \ddot{\hat{x}}_{1ref} - \dot{\hat{d}}_1 - \hat{d}_2 \\ &\quad -H_{s1}\mathrm{sgn}(s_1) - H_{s2}s_1 && (52) \end{aligned}$$

$$\begin{aligned} h_2 &= -a_2\left(e_{x4} - \dot{\hat{x}}_{3ref}\right) + \ddot{\hat{x}}_{3ref} - \dot{\hat{d}}_3 - \hat{d}_4 \\ &\quad -H_{s3}\mathrm{sgn}(s_2) - H_{s4}s_2 && (53) \end{aligned}$$

where $H_{s1}$ to $H_{s4}$ represent the gains of positive definite sliding mode controller. To sum up, the convergence and stability of the controller can be obtained by the following theorem:

**Theorem 1**: If the following condition is satisfied: 1) $(H_{s1} - H_{s2}|s_1|) > (1+a_1)\sigma_d$ and $(H_{s3} - H_{s4}|s_2|) > (1+a_2)\sigma_d$; 2) a sufficiently large $H_{\min}$ is selected, the energy interaction converter based on equations (28)-(29) is asymptotically stable, and its output voltage $V_{out}$ can track up to $V_{ref}$.

*Proof*: Applying equations (22)-(25), (39)-(42) and (46)-(49), the derivatives of slip surfaces $s_1$ and $s_2$ are shown as follows:

$$\begin{aligned} \dot{s}_1 &= a_1 e_{d1} + e_{d2} - H_{s1}\mathrm{sgn}(s_1) - H_{s2}s_1 \quad (54)\\ \dot{s}_2 &= a_2 e_{d3} + e_{d4} - H_{s3}\mathrm{sgn}(s_2) - H_{s4}s_2 \quad (55)\end{aligned}$$

Define the standard Lyapunov equation:

$$V(s_1, s_2) = 0.5s_1^2 + 0.5s_2^2 \quad (56)$$

Based on this, the derivative of $V = V(s_1, s_2)$ is shown as follows:

$$\begin{aligned} \dot{V} &= s_1\dot{s}_1 + s_2\dot{s}_2\\ &= -H_{s1}|s_1| - H_{s2}s_1^2 - H_{s3}|s_3| - H_{s4}s_2^2\\ &\quad + (a_1 e_{d1} + e_{d2})s_1 + (a_2 e_{d3} + e_{d4})s_2\\ &\le -H_{s1}|s_1| - H_{s2}s_1^2 - H_{s3}|s_3| - H_{s4}s_2^2\\ &\quad + (1+a_1)\sigma_d s_1 + (1+a_2)\sigma_d s_2\\ &= -[H_{s1} + H_{s2}|s_1| - (1+a_1)\sigma_d]|s_1|\\ &\quad - [H_{s3} + H_{s4}|s_2| - (1+a_2)\sigma_d]|s_2| \quad (57)\end{aligned}$$

Therefore, if $(H_{s1} - H_{s2}|s_1|) > (1+a_1)\sigma_d$ and $(H_{s3} - H_{s4}|s_2|) > (1+a_2)\sigma_d$, the state error of the system converges asymptotically to the defined sliding surfaces $s_1 = 0$ and $s_2 = 0$. When $H_{d1}$ to $H_{d4}$ is large enough, $\sigma_d$ can be arbitrarily small, and $H_{s1}$ to $H_{s4}$ can also be selected to be relatively small to alleviate the sliding mode chattering problem. Based on equations (50)-(51), if $s_1 = 0$ and $s_2 = 0$, let

$$\begin{aligned} e_{x2} &= -a_1 e_{x1} + \dot{\hat{x}}_{1ref} \quad (58)\\ e_{x4} &= -a_2 e_{x3} + \dot{\hat{x}}_{3ref} \quad (59)\\ \dot{e}_{x1} &= e_{x2} + e_{d1} - \dot{\hat{x}}_{1ref} \quad (60)\\ \dot{e}_{x3} &= e_{x4} + e_{d3} - \dot{\hat{x}}_{3ref} \quad (61)\end{aligned}$$

By substituting equations (57)-(58) into equations (59)-(60) and combining equations (39)-(42), it can be seen that the sliding mode dynamics of the energy interaction converter based on disturbance observer is shown as follows:

$$\dot{e} = \mathbf{A}e + \mathbf{B}\dot{d} \quad (62)$$

where $\dot{e} = [\dot{e}_{x1}, \dot{e}_{d1}, \dot{e}_{d2}, \dot{e}_{x3}, \dot{e}_{d3}, \dot{e}_{d4}]^T$ and $\dot{d} = \left[\dot{d}_1, \dot{d}_2, \dot{d}_3, \dot{d}_4\right]$. $\mathbf{A}$ and $\mathbf{B}$ are shown as follows:

$$\mathbf{A} = \begin{bmatrix} -a_1 & 1 & 0 & 0 & 0 & 0\\ 0 & -H_{d1} & 0 & 0 & 0 & 0\\ 0 & 0 & -H_{d2} & 0 & 0 & 0\\ 0 & 0 & 0 & -a & 1 & 0\\ 0 & 0 & 0 & 0 & -H_{d3} & 0\\ 0 & 0 & 0 & 0 & 0 & -H_{d4} \end{bmatrix}$$

$$\mathbf{B} = \begin{bmatrix} 0 & 0 & 0 & 0\\ 1 & 0 & 0 & 0\\ 0 & 1 & 0 & 0\\ 0 & 0 & 0 & 0\\ 0 & 0 & 1 & 0\\ 0 & 0 & 0 & 1 \end{bmatrix}$$

Define the following Lyapunov equation:

$$V_e = Q(e_{di}) + 0.5e_{x1}^2 + 0.5e_{x3}^2 \quad (63)$$

Its derivative is shown below

$$\begin{aligned} \dot{V}_e &= \dot{Q}(e_{di}) + e_{x1}\dot{e}_{x1} + e_{x3}\dot{e}_{x3}\\ &= \dot{Q}(e_{di}) + \left(-a_1 e_{x1}^2 + e_{x1}e_{d1}\right) + \left(-a_3 e_{x3}^2 + e_{x3}e_{d3}\right)\\ &= \sum_{i=1}^{4}\left(-H_{di}e_{di}^2 + e_{di}\dot{d}_i\right) + \left(-a_1 e_{x1}^2 + e_{x1}e_{d1}\right)\\ &\quad + \left(-a_3 e_{x3}^2 + e_{x3}e_{d3}\right) \quad (64)\end{aligned}$$

Using Young inequality, the following equations can be obtained

$$\begin{aligned} \dot{V}_e &\le -(H_{d1} - 1)e_{d1}^2 - H_{d2}e_{d2}^2 - (H_{d3} - 1)e_{d3}^2 - H_{d4}e_{d4}^2\\ &\quad - (a_1 - 0.5)e_{x1}^2 - (a_3 - 0.5)e_{x3}^2 + 0.5\sum_{i=1}^{4}\dot{d}_i \quad (65)\end{aligned}$$

Considering the equation (62), the inequation (64) can be rewritten as follows:

$$\dot{V}_e \le -H_{\min}V_e + 2\tilde{d}_{\max} \quad (66)$$

where $H_{\min} = \min\left[\begin{array}{c} 2(H_{d1} - 1), 2H_{d2}, 2(H_{d3} - 1),\\ 2H_{d4}, 2(a_1 - 0.5), 2(a_2 - 0.5) \end{array}\right] > 0$ and $\tilde{d}_{\max} = \max\left[\tilde{d}_{1\max}, \tilde{d}_{2\max}, \tilde{d}_{3\max}, \tilde{d}_{4\max}\right]$. According to the equation (65), $V_e$ is bounded and $V_e \le \xi$ in a finite amount of time. Through selecting a large enough $H_{\min}$, it can ensure that $V_e$ tends to zero. Therefore, the error defined through the equation (61) can converge to any small neighborhood of the original system. As a result, the theorem is proved.

To sum up, the output voltage of the upper/lower arm of the energy interaction converter can be well controlled to $V_u = V_b = V_{ref}^*$, in other word, the output voltage of the energy interaction converter can achieve $V_{out} = V_{ref}$.

## IV. Current inner loop proportional-resonant controller

According to the fixed power and voltage, the output current of the upper arm or below arm regarding the energy interaction converter is fixed ($i_u = i_b = C$). Based on this, the heat loss of the energy interaction converter is $P_{loss} = 0.5\left(i_{u1}^2R + i_{u2}^2R + i_{u3}^2R + i_{b1}^2R + i_{b2}^2R + i_{b3}^2R\right)$. If $i_{u1} = i_{u2} = i_{u3} = 1/3C$ and $i_{b1} = i_{b2} = i_{b3} = 1/3C$, the heat loss of the energy interaction converter is minimum in light of the inequality of arithmetic and geometric means. Therefore, the current sharing modular controller should be proposed to make $i_{u1} = i_{u2} = i_{u3} = 1/3C$ and $i_{b1} = i_{b2} = i_{b3} = 1/3C$. Although the arms of the energy interaction converter are mirror symmetrical, the inevitable deviation of circuit parameters and duty cycle will lead to the inconsistency of current flowing through the six channels, resulting in unnecessary loss and heating of hardware device. Traditionally, PI controller is always used to realize accurate current sharing. Nevertheless, the constant power load is prone to low frequency and sub-synchronous oscillation in electromagnetic timescale. Thus, the current sharing proportional-resonance (PR) controller is adopted in this paper. The detailed control block diagram is shown in Fig. 5 where $i_{ave} = (i_u + i_b)/6$. Meanwhile, the

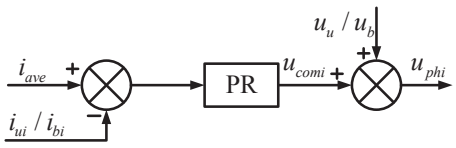


Fig. 5: Current sharing PR controller.

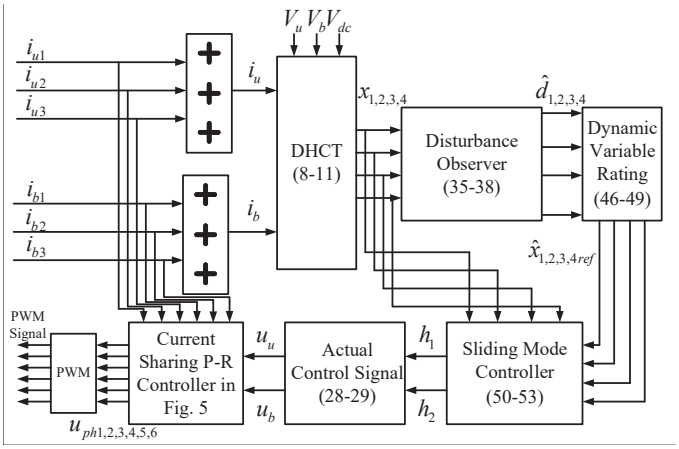


Fig. 6: Overall control block diagram.

current sharing compensator for each path is expressed as follows:

$$u_{comi} = K_P e_{comi} + \frac{K_R s}{s^2 + \omega_c^2} e_{comi} \tag{67}$$

where $e_{comi} = i_{ave} - i_{ui}$ or $e_{comi} = i_{ave} - i_{bi}$; $K_P$ and $K_R$ represent proportional parameter and resonant parameter, respectively. Meanwhile, $K_P > 0$ and $K_R > 0$. Noting that the control bandwidth of sliding mode controller is more than 5 times higher than that of proportional resonant controller [28]. For pure dc current without low-frequency oscillation, PI controller is widely applied, and under this case, $\omega_c = 0$. In the system with weak source and constant power load, low-frequency oscillation whose frequency is below than 5 Hz, should be considered [29]-[30]. In order to improve performance for these low-frequency components (1 to 5 Hz), $\omega_c$ is selected as $\omega_c = (1+5)/2 = 3Hz$ in this paper. Of course, the plenty of PR controllers ($\omega_i = i$) can be applied to further improve the controller performance.

To sum up, the overall control block diagram of the vehicle-vehicle energy interaction converter is shown in Fig. 6.

## V. Simulation

The effectiveness of the energy interaction converter controlled through disturbance observer based sliding mode control algorithm is verified by simulation results in this section. In Cases 1-3, the different rated voltage or power vehicles are applied to verify the high application of the proposed method. Furthermore, Case 4 is applied to illustrate the high performance of the proposed method. The selection regarding controller parameter values can be divided into two parts, i.e., PR controller and disturbance observer based sliding model controller. Firstly, in the system with weak source and constant power load, the low-frequency oscillation whose frequency is

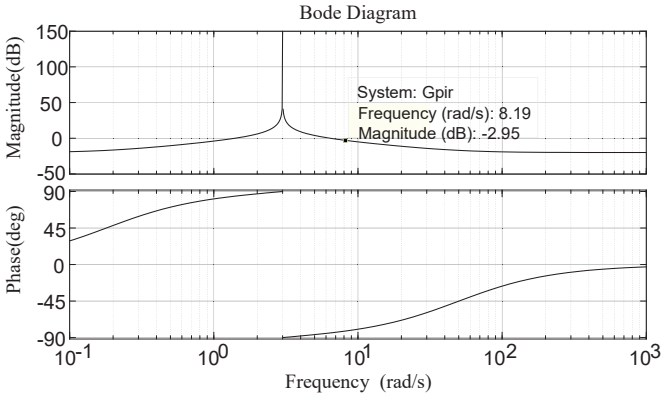


Fig. 7: Bode diagram of the PR controller.

below than 5 Hz, should be considered [29]-[30]. In order to improve performance for these low-frequency components (1 to 5 Hz), $\omega_c$ is selected as 3 Hz in this paper. Secondly, the interactive impact between two controllers can be ignored if the control bandwidth of one controller is more than 5 times higher that of another controller [26]. Therein, the control bandwidth of sliding mode controller is more than 100 Hz. In order to eliminate the interactive impact between two controllers, the control bandwidth of the proposed PR controller should be below than 20 Hz. Based on this, $K_P$ and $K_R$ are selected as $K_P = 0.1$ and $K_R = 5$. As shown in Fig. 7, the control bandwidth of the proposed PR controller is below than 10 Hz. Thirdly, the parameters of disturbance observer based sliding model controller is selected through **Theorem 1**. Under this case, the conditions $((H_{s1} - H_{s2}|s_1|) > (1+a_1)\sigma_d$ and $(H_{s3} - H_{s4}|s_2|) > (1+a_2)\sigma_d)$ should be satisfied, and one sufficiently large $H_{min}$ should be selected. Firstly, since one sufficiently large $H_{min}$ should be selected, $H_{d1}$ to $H_{d4}$ should be selected as big as possible. Based on this, $H_{d1}$ to $H_{d4}$ can be chosen as $H_{d1} = H_{d3} = 2000$ and $H_{d2} = H_{d4} = 280$. Considering $H_{s1}$ and $H_{s3}$ are positive definite switching gains, which causes the sliding mode controller chattering problem, small $H_{s1}$ and $H_{s3}$ should be chosen. As a result, $H_{s1}$ and $H_{s3}$ can be chosen as $H_{s1} = H_{s3} = 0.01$. Meanwhile, since $H_{s2}$ and $H_{s4}$ can decrease the voltage dip during the load power change, big $H_{s2}$ and $H_{s4}$ should be chosen. As a result, $H_{s2}$ and $H_{s4}$ can be chosen as $H_{s2} = H_{s4} = 20000$. Since $a_1$ and $a_2$ can decrease the voltage dip during the load power change, big $a_1$ and $a_2$ should be chosen. However, the conditions $((H_{s1} - H_{s2}|s_1|) > (1+a_1)\sigma_d$ and $(H_{s3} - H_{s4}|s_2|) > (1+a_2)\sigma_d)$ should be satisfied. Hence, $a_1$ and $a_2$ can be chosen as $a_1 = a_2 = 10000$. Noting that the red line represents the rated reference value in following simulation test system.

### A. Case 1

The practical output voltage of the energy supply vehicle B is $75V$, and the ideal voltage of the energy consumption vehicle A is $300V$ and its capacity is $P_{CPL} = 30kW$. Based on this, the ideal output voltage of the upper/lower bridge arm of the energy interaction converter is $V_{ref}^* =$

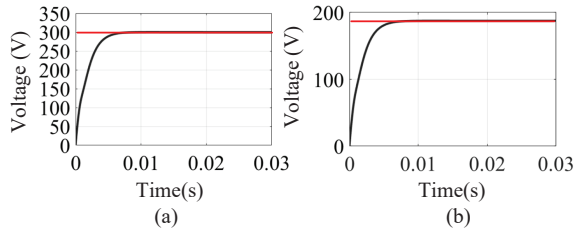


Fig. 8: The voltage of the energy interaction converter under Case 1: (a) actual output voltage; (b) actual output voltage of upper/lower bridge arm.

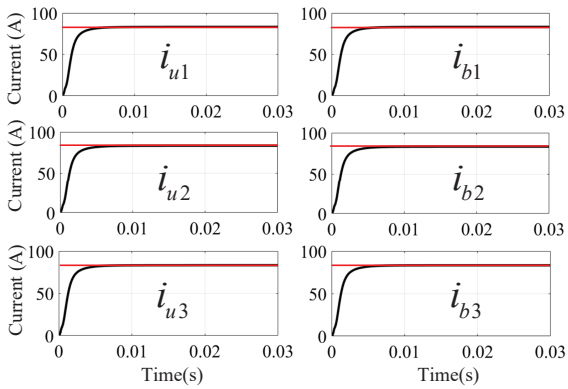


Fig. 9: Each bridge arm current of the energy interaction converter under Case 1.

$(V_{ref}+V_{dc})/2 = 187.5V$, and the ideal output voltage of the energy interaction converter is $V_{ref} = 300V$. From Fig. 8(a), the actual output voltage of the energy interaction converter is $V_{out} = 300V$. From Fig. 8(b), the actual output voltage of the upper/lower bridge arm of the energy interaction converter is $V_u = V_b = (V_{ref}+V_{dc})/2 = 187.5V$. Based on this, the energy interaction converter controlled through disturbance observer based sliding mode control algorithm can provide ideal voltage for the energy consumption vehicle A. Furthermore, the current of each arm regarding energy interaction converter is same, which is shown in Fig. 9. The performance of the current sharing PR controller can be ensured. As a result, the effectiveness of the energy interaction converter controlled through disturbance observer based sliding mode control algorithm has been verified by foresaid simulation results.

### B. Case 2

The practical output voltage of the energy supply vehicle B is $60V$, and the ideal voltage of the energy consumption vehicle A is also $300V$ and its capacity is also $P_{CPL} = 30kW$. To this end, the ideal output voltage of the upper/lower bridge arm of the energy interaction converter is $V^*_{ref} = (V_{ref}+V_{dc})/2 = 180V$, and the ideal output voltage of the energy interaction converter is $V_{ref} = 300V$. The actual output voltage of the energy interaction converter is $V_{out} = 300V$, which is shown in Fig, 10(a). As shown in Fig. 10(b), the actual output voltage of the upper/lower bridge arm of the energy interaction converter is $V_u = V_b = (V_{ref}+V_{dc})/2 = 180V$. To this end, the energy interaction converter controlled through

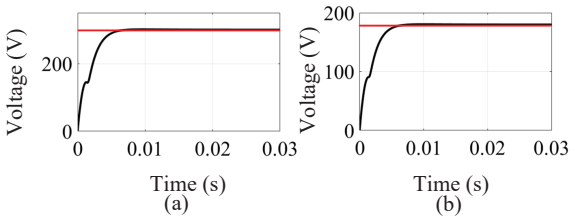


Fig. 10: The voltage of the energy interaction converter under Case 2: (a) actual output voltage; (b) actual output voltage of upper/lower bridge arm.

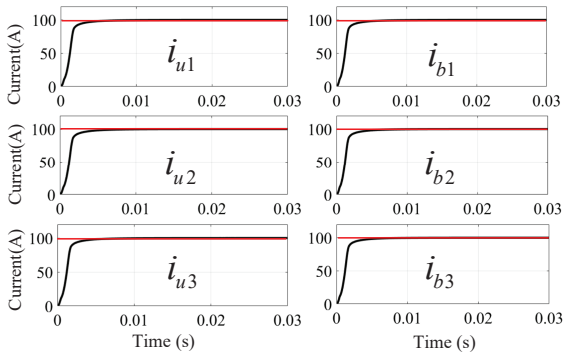


Fig. 11: Each bridge arm current of the energy interaction converter under Case 2.

disturbance observer based sliding mode control algorithm can provide ideal voltage for the energy consumption vehicle A. This conclusion is the same as the conclusion in Case 1. Furthermore, the current of each arm regarding energy interaction converter is also same, which is shown in Fig. 11. The effectiveness of the current sharing PR controller can be also ensured. As a result, the effectiveness of the energy interaction converter controlled through disturbance observer based sliding mode control algorithm has been verified by foresaid simulation results.

### C. Case 3

The practical output voltage of the energy supply vehicle B is $60V$, and the ideal voltage of the energy consumption vehicle A is chosen as $250V$ and its capacity is also $P_{CPL} = 20kW$. To that end, the ideal output voltage of the upper/lower bridge arm of the energy interaction converter is $V^*_{ref} = (V_{ref}+V_{dc})/2 = 155V$, and the ideal output voltage of the energy interaction converter is $V_{ref} = 250V$. The actual output voltage of the energy interaction converter is $V_{out} = 250V$, which is shown in Fig, 12(a). As shown in Fig. 12(b), the actual output voltage of the upper/lower bridge arm of the energy interaction converter is $V_u = V_b = (V_{ref}+V_{dc})/2 = 155V$. Thus, the energy interaction converter controlled through disturbance observer based sliding mode control algorithm can provide ideal voltage for the energy consumption vehicle A. This conclusion is the same as the conclusion in Cases 1 and 2. Furthermore, the current of each arm regarding energy interaction converter is also same, which is shown in Fig. 13. The effectiveness of the current sharing PR controller can be ensured. Therefore, the effectiveness of

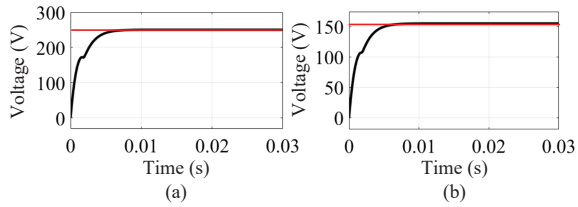


Fig. 12: The voltage of the energy interaction converter under Case 3: (a) actual output voltage; (b) actual output voltage of upper/lower bridge arm.

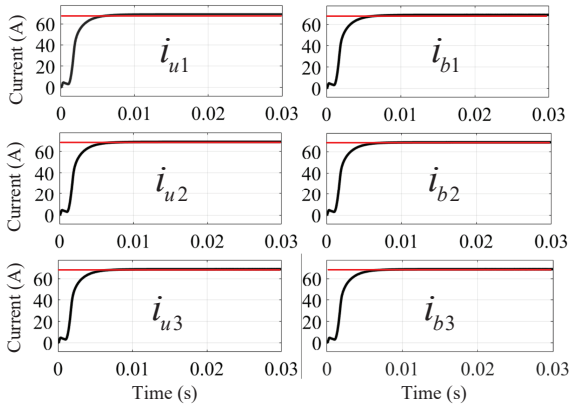


Fig. 13: Each bridge arm current of the energy interaction converter under Case 3.

the energy interaction converter controlled through disturbance observer based sliding mode control algorithm has been verified by foresaid simulation results.

### D. Case 4

In order to verify the high performance of the proposed method under different voltage and current of the battery charging, some simulation results are provided, which are shown as follows: Firstly, the ideal voltage of the energy consumption vehicle A is 300V at initial time, and the ideal voltage of the energy consumption vehicle A is 250V at 0.015s. As shown in Fig. 14, the actual output voltage of the energy interaction converter is same as the ideal voltage. Wherein, the main observation values are $\hat{d}_1$ and $\hat{d}_3$. Thus, the time-domain curve of the real values and estimation values regarding $\hat{d}_1$ and $\hat{d}_3$ are shown in Figs 15-16. As shown in Figs. 15-16, the observation accuracy can be verified. Furthermore, the ideal voltage of the energy consumption vehicle A is 300V. Therein, the capacity of the energy consumption vehicle A is 20kW at initial time, and the capacity of the energy consumption vehicle A is 30kW at 0.015s. As shown in Fig. 17, the actual output voltage of the energy interaction converter is same as the ideal voltage. Based on this, the high performance of the proposed method under different voltage and current of the battery charging can be verified.

In order to illustrate the performance of the proposed method, one comparison research involves the proposed method and the traditional sliding mode control method, which is shown through (50)-(51). Fig. 18 shows the actual output voltage of the energy interaction converter regulated by the

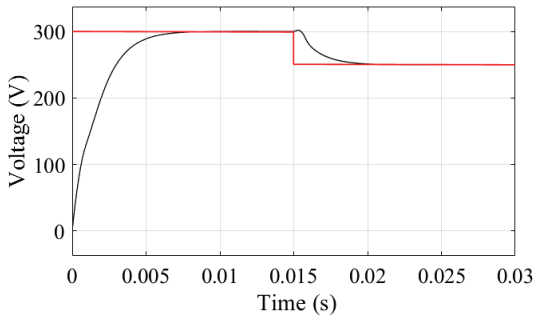


Fig. 14: The actual output voltage of the energy interaction converter under different voltage case.

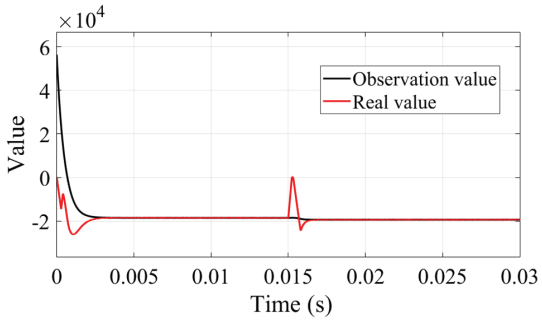


Fig. 15: The relative curves between observation value $\hat{d}_1$ and real value.

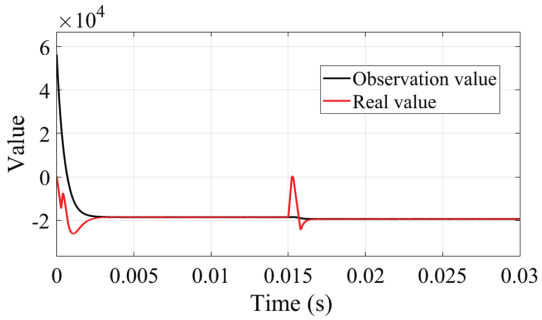


Fig. 16: The relative curves between observation value $\hat{d}_3$ and real value.

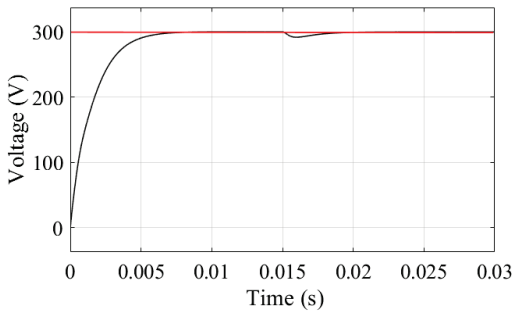


Fig. 17: The actual output voltage of the energy interaction converter under different capacity case.

proposed method (in black) and the traditional sliding mode control method (in blue). Therein, the ideal voltage of the energy consumption vehicle A is 300V. Furthermore, the

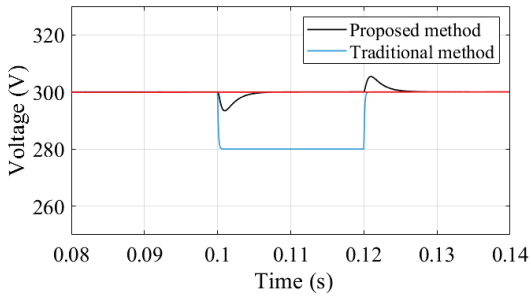


Fig. 18: The actual output voltages of the energy interaction converter obtained through using the proposed method and the traditional method.

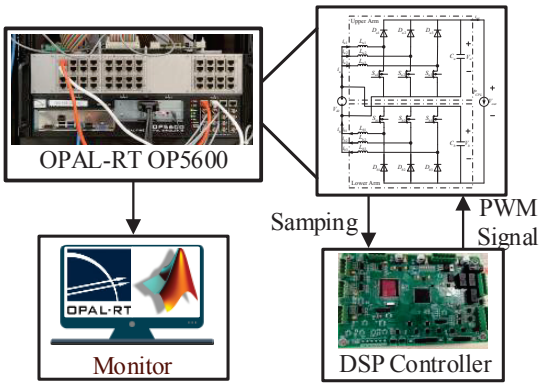


Fig. 19: The CHIL experiment topology.

capacity of the energy consumption vehicle A is form 30kW to 40kW at 0.1s, and restores to 30kW at 0.12s. Although the values of $x_{2ref}$ and $x_{4ref}$ are selected to satisfy the conditions of $d_1+x_{2ref}=0$ and $d_2+x_{4ref}=0$ under 30kW, the change regarding 40kW causes an error. As a result, the actual output voltage of the energy interaction converter is 280V from 0.1s to 0.12s, which is controlled through the traditional method. However, the actual output voltage of the energy interaction converter is 300V, which is controlled through the proposed method. Based on this, the high performance of the proposed method can be verified.

## VI. Experiment

In order to verify the high application of the energy interaction converter controlled through disturbance observer based sliding mode control algorithm for vehicles, the controller hardware-in-the-loop (CHIL) experiments are executed in OPAL-RT real-time simulation system with the system parameters, which are the same as the simulation section. The CHIL experiment facility is cited in our previous literature [28]. The detailed experimental figure is shown in Fig. 19. Therein, the control frequency is $10^5 Hz$, and the energy interaction converter is controlled through Digital Signal Processor (DSP) controllers (TMS320F28335). The inputs of DSP are current ($i_u$ and $i_b$) and voltage ($V_u$, $V_b$ and $V_{dc}$) measurements, which are converted from digital signals to the analog signals by the D2A terminals of OPAL-RT system. Furthermore, the outputs of the DSP controllers are pulsewidth modulation (PWM) signals, which are sent to the PWM channels of the OPAL-RT system and then drive the power switches in the energy interaction converter model. Finally, the energy interaction converter model is embedded into OPAL-RT OP5600 simulator. Noting that the red line represents the rated reference value in following simulation test system. The practical output voltage of the energy supply vehicle B is $75V$, and the ideal voltage of the energy consumption vehicle A is $300V$ and its capacity is $P_{CPL}=30kW$. Therefore, the ideal output voltage of the energy interaction converter is $V_{ref}=300V$. From Fig. 20, the actual output voltage of the energy interaction converter is $V_{out}=300V$. As a result, the energy interaction converter controlled through disturbance observer based sliding mode control algorithm can provide ideal voltage for the energy consumption vehicle

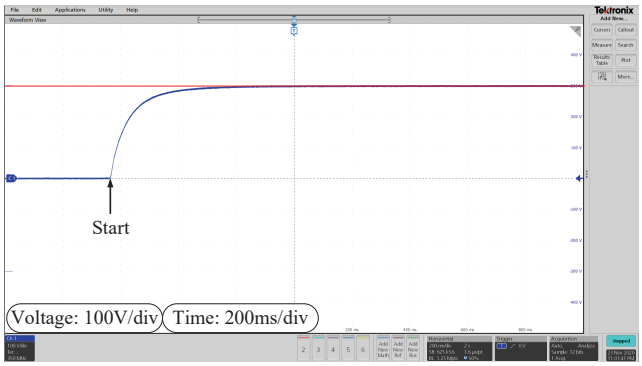


Fig. 20: The actual output voltage of the energy interaction converter under CHIL experiment.

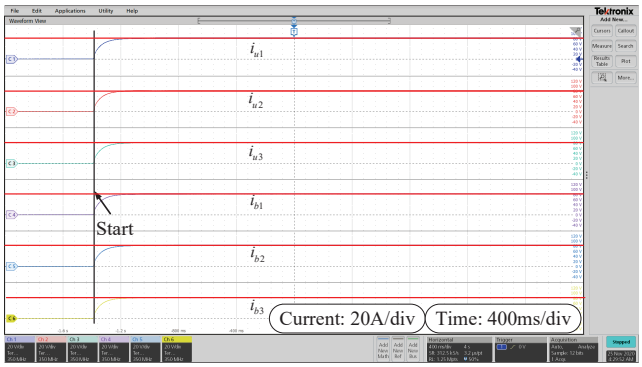


Fig. 21: Each bridge arm current of the energy interaction converter under CHIL experiment.

A. Furthermore, the current of each arm regarding energy interaction converter is same, which is shown in Fig. 21. The performance of the current sharing PR controller can be ensured. As a result, the effectiveness of the energy interaction converter controlled through disturbance observer based sliding mode control algorithm has been verified by the relative experimental results.

## VII. Conclusion

In order to solve the two main problems which hinder the development of electric vehicles, i.e., charger unavailability and range anxiety, this paper has proposed the energy interaction converter controlled through disturbance observer based

sliding mode control algorithm such that the owner can realize the fast energy mutual assistance between vehicle and vehicle. In view of the low minimum short circuit ratio and high power density, the equivalent six channel interleaved floating dual boost converter and its state-space function have been firstly constructed in this paper. For weak source and constant power load, the disturbance observer based sliding mode control algorithm based on the built state-space function has been proposed to provide constant voltage and power which are in line with the relative standard of electric vehicles. In order to solve the problem of six channel current sharing, the current sharing PR controller has been designed to reduce the heat loss and improve the service life of device. Finally, the simulation and experiment results have been provided to illustrate that the proposed energy interaction converter controlled through disturbance observer based sliding mode control algorithm is effective.

## REFERENCES


[1] Schfer B., Beck C., Aihara K., Witthaut D. and Timme M. "Non-gaussian power grid frequency fluctuations characterized by lévy-stable laws and superstatistics," *Nature Energy*, vol. 3, pp. 119-126, Jan. 2018.

[2] Y. Jia, R. Jibrin and D. Gorges, "Energy-Optimal Adaptive Cruise Control for Electric Vehicles based on Linear and Nonlinear Model Predictive Control," *IEEE Transactions on Vehicular Technology,* doi: 10.1109/TVT.2020.3044265.

[3] J. Wang, Y. Cai, L. Chen, D. Shi, S. Wang and Z. Zhu, "Research on Compound Coordinated Control for A Power-split Hybrid Electric Vehicle Based on Compensation of Non-ideal Communication Network," *IEEE Transactions on Vehicular Technology,* doi: 10.1109/TVT.2020.3040777.

[4] Yanyan Xu, Serdar Colak, Emre C. Kara, Scott J. Moura and Marta C. González, "Planning for electric vehicle needs by coupling charging profiles with urban mobility," *Nature Energy*, vol. 3, pp. 484-493, April, 2018.

[5] C. Zhai, F. Luo and Y. Liu, "A Novel Predictive Energy Management Strategy for Electric Vehicles Based on Velocity Prediction," *IEEE Transactions on Vehicular Technology*, vol. 69, no. 11, pp. 12559-12569, Nov. 2020.

[6] R. Wang, Q. Sun, D. Qin, Y. Li, X. Li and P. Wang, "Steady-state Stability Assessment of AC-busbar Plug-in Electric Vehicle Charging Station with Photovoltaic," *Journal of Modern Power Systems and Clean Energy*, vol. 8, no. 5, pp. 884-894, September 2020.

[7] W. Jiang, X. Zhang, F. Guo, J. Chen, P. Wang and L. H. Koh, "Large-Signal Stability of Interleave Boost Converter System With Constant Power Load Using Sliding-Mode Control," *IEEE Transactions on Industrial Electronics*, vol. 67, no. 11, pp. 9450-9459, Nov. 2020.

[8] R. Wang, Q. Sun, D. Ma, D. Qin, Y. Gui and P. Wang, "Line Inductance Stability Operation Domain Assessment for Weak Grids With Multiple Constant Power Loads," *IEEE Transactions on Energy Conversion*, doi: 10.1109/TEC.2020.3021070

[9] M. Cespedes, L. Xing and J. Sun, "Constant-Power Load System Stabilization by Passive Damping," *IEEE Transactions on Power Electronics*, vol. 26, no. 7, pp. 1832-1836, July 2011.

[10] N. Kumar, M. Mohamadi and S. K. Mazumder, "Passive Damping Optimization of the Integrated-Magnetics-Based Differential-Mode Ćuk Rectifier," *IEEE Transactions on Power Electronics*, vol. 35, no. 10, pp. 10008-10012, Oct. 2020.

[11] D. Yang, J. Qin, Y. Pang and T. Huang, "A Novel Double-Stacked Autoencoder for Power Transformers DGA Signals with Imbalanced Data Structure," *IEEE Transactions on Industrial Electronics*, doi: 10.1109/TIE.2021.3059543.

[12] Y. Liu, D. Jin, S. Jiang, W. Liang, J. Peng and C. Lai, "An Active Damping Control Method for the LLCL Filter-Based SiC MOSFET Grid-Connected Inverter in Vehicle-to-Grid Application," *IEEE Transactions on Vehicular Technology*, vol. 68, no. 4, pp. 3411-3423, April 2019.

[13] S. Singh, A. R. Gautam, and D. Fulwani, "Constant power loads and their effects in dc distributed power systems: A review," *Renewable and Sustainable Energy Reviews*, vol. 72, pp. 407-421, 2017.

[14] J. A. Solsona, S. G. Jorge and C. A. Busada, "Nonlinear Control of a Buck Converter Which Feeds a Constant Power Load," *IEEE Transactions on Power Electronics*, vol. 30, no. 12, pp. 7193-7201, Dec. 2015.

[15] G. Sulligoi, D. Bosich, G. Giadrossi, L. Zhu, M. Cupelli and A. Monti, "Multiconverter Medium Voltage DC Power Systems on Ships: Constant-Power Loads Instability Solution Using Linearization via State Feedback Control," *IEEE Transactions on Smart Grid*, vol. 5, no. 5, pp. 2543-2552, Sept. 2014.

[16] S. Arora, P. Balsara and D. Bhatia, "Input-Output Linearization of a Boost Converter With Mixed Load (Constant Voltage Load and Constant Power Load)," *IEEE Transactions on Power Electronics*, vol. 34, no. 1, pp. 815-825, Jan. 2019.

[17] N. Guo, X. Zhang, Y. Zou, B. Lenzo and T. Zhang, "A Computationally Efficient Path-Following Control Strategy of Autonomous Electric Vehicles With Yaw Motion Stabilization," *IEEE Transactions on Transportation Electrification*, vol. 6, no. 2, pp. 728-739, June 2020.

[18] N. Guo, B. Lenzo, X. Zhang, Y. Zou, R. Zhai and T. Zhang, "A Real-Time Nonlinear Model Predictive Controller for Yaw Motion Optimization of Distributed Drive Electric Vehicles," *IEEE Transactions on Vehicular Technology*, vol. 69, no. 5, pp. 4935-4946, May 2020.

[19] Y. Zhao, W. Qiao, and D. Ha, "A sliding-mode duty-ratio controller for dc/dc buck converters with constant power loads,*IEEE Transactions on Industry Applications*, vol. 50, no. 2, pp. 1448-1458, 2014.

[20] S. Singh, D. Fulwani, and V. Kumar, "Robust sliding-mode control of dc/dc boost converter feeding a constant power load, *IET Power Electronics*, vol. 8, no. 7, pp. 1230-1237, 2015.

[21] Y. Huangfu, S. Zhuo, F. Chen, S. Pang, D. Zhao and F. Gao, "Robust Voltage Control of Floating Interleaved Boost Converter for Fuel Cell Systems," *IEEE Transactions on Industry Applications*, vol. 54, no. 1, pp. 665-674, Jan.-Feb. 2018.

[22] H. Wu, V. Pickert, D. Giaouris and B. Ji, "Nonlinear Analysis and Control of Interleaved Boost Converter Using Real-Time Cycle to Cycle Variable Slope Compensation," *IEEE Transactions on Power Electronics*, vol. 32, no. 9, pp. 7256-7270, Sept. 2017.

[23] W. Rui, S. Qiuye, M. Dazhong and H. Xuguang, "Line Impedance Cooperative Stability Region Identification Method for Grid-Tied Inverters Under Weak Grids," *IEEE Transactions on Smart Grid*, vol. 11, no. 4, pp. 2856-2866, July 2020.

[24] W. Wu et al., "Sequence Impedance Modeling and Stability Comparative Analysis of Voltage-Controlled VSGs and Current-Controlled VSGs," *IEEE Transactions on Industrial Electronics*, vol. 66, no. 8, pp. 6460-6472, Aug. 2019.

[25] P. Krishayya, R. Adapa, M. Holm., "IEEE guide for planning DC links terminating at AC locations having low short-circuit capacities, part I: AC/DC system interaction phenomena," *CIGRE, France*, 1997.

[26] R. Wang, Q. Sun, X. Liu and D. Ma, "Power flow calculation based on local controller impedance features for the AC microgrid with distributed generations," *IET Energy Systems Integration*, vol. 1, no. 3, pp. 202-209, 9 2019.

[27] X. Xu, Q. Liu, C. Zhang and Z. Zeng, "Prescribed Performance Controller Design for DC Converter System With Constant Power Loads in DC Microgrid," *IEEE Transactions on Systems, Man, and Cybernetics: Systems*, vol. 50, no. 11, pp. 4339-4348, Nov. 2020.

[28] W. Rui, S. Qiuye, Z. Pinjia, G. Yonghao, Q. Dehao and W. Peng, "Reduced-Order Transfer Function Model of the Droop-Controlled Inverter via Jordan Continued-Fraction Expansion," *IEEE Transactions on Energy Conversion*, vol. 35, no. 3, pp. 1585-1595, Sept. 2020.

[29] R. Wang, Q. Sun, D. Ma and Z. Liu, "The Small-Signal Stability Analysis of the Droop-Controlled Converter in Electromagnetic Timescale," *IEEE Transactions on Sustainable Energy*, vol. 10, no. 3, pp. 1459-1469, July 2019.

[30] H. Wang, W. Mingli and J. Sun, "Analysis of Low-Frequency Oscillation in Electric Railways Based on Small-Signal Modeling of Vehicle-Grid System in dq Frame," *IEEE Transactions on Power Electronics*, vol. 30, no. 9, pp. 5318-5330, Sept. 2015.

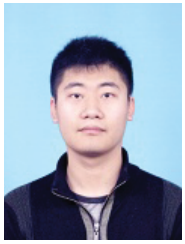

**Rui Wang** received the B.S. degree in electrical engineering and automation in 2016 from Northeastern University, Shenyang, China, where he received the Ph.D. degree in power electronics and power drive in 2021. He is a lecturer in Northeastern University. He has authored or coauthored over 50 papers, authorized over 20 invention patents His research interest focuses on collaborative optimization of distributed generation and its stability analysis of electromagnetic timescale in cyber-energy syetem.

**Qiuye Sun** (M'11-SM'19) received the Ph.D. degree in 2007. He is currently a full Professor with Northeastern University and obtained Special Government Allowances from the State Council in China. He has authored or coauthored over 200 papers, authorized over 100 invention patents, and published over 10 books or textbooks. He is an Associate Editor of IEEE Trans NNLS, IET Cyber-Physical Systems, CSEE Journal of Power and Energy Systems, IEEE/CAA Journal of Automatica Sinica and so on. His current research interests include optimization analysis technology of power distribution network, network control of Energy Internet, Integrated Energy Systems and Microgrids.

**Chenghao Sun** received the B.S. degree and the M.Sc. degree in 2017 and 2019 from Northeastern University, Shenyang, China, where he is currently working toward the Ph.D. degree. His current research interests include modeling, modulation strategy and synchronous rectification of resonant converters, etc.

**Huaguang Zhang** (F'14) received the B.S. degree and the M.S. degree in control engineering from Northeast Dianli University of China, Jilin City, China, in 1982 and 1985, respectively. He received the Ph.D. degree in thermal power engineering and automation from Southeast University, Nanjing, China, in 1991. He joined the Department of Automatic Control, Northeastern University, Shenyang, China, in 1992, as a Postdoctoral Fellow for two years. Since 1994, he has been a Professor and Head of the Institute of Electric Automation, School of Information Science and Engineering, Northeastern University, Shenyang, China. His main research interests are fuzzy control, stochastic system control, neural networks based control, nonlinear control, and their applications. He has authored and coauthored over 280 journal and conference papers, six monographs and co-invented 90 patents.

Dr. Zhang is the fellow of IEEE, the E-letter Chair of IEEE CIS Society, the former Chair of the Adaptive Dynamic Programming & Reinforcement Learning Technical Committee on IEEE Computational Intelligence Society. He is an Associate Editor of AUTOMATICA, IEEE TRANSACTIONS ON NEURAL NETWORKS, IEEE TRANSACTIONS ON CYBERNETICS, and NEUROCOMPUTING, respectively. He was an Associate Editor of IEEE TRANSACTIONS ON FUZZY SYSTEMS (2008-2013). He was awarded the Outstanding Youth Science Foundation Award from the National Natural Science Foundation Committee of China in 2003. He was named the Cheung Kong Scholar by the Education Ministry of China in 2005. He is a recipient of the IEEE Transactions on Neural Networks 2012 Outstanding Paper Award.

**Yonghao Gui** (S'11-M'17-SM'20) received the B.S. degree in automation from Northeastern University, Shenyang, China, in 2009, and the M.S. and Ph.D. degrees in electrical engineering from Hanyang University, Seoul, South Korea, in 2012 and 2017, respectively. From Feb. 2017 to Nov. 2018, he worked with the Department of Energy Technology, Aalborg University, Aalborg, Denmark, as a Postdoctoral Researcher. Since Dec. 2018, he has been working with the Automation Control Section, Department of Electronic Systems, Aalborg University, Aalborg, Denmark, where he is currently an Assistant Professor. His research interests include Control of Power Electronics in Power Systems, Energy Internet, and Smart Grids.

Dr. Gui has served as an Associate Editor for the IEEE Transaction on Energy Conversion, IEEE Access, and International Journal of Control, Automation and Systems (IJCAS). He was a recipient of the IEEE Power & Energy Society General Meeting Best Conference Paper Award in 2019 and the IJCAS Academic Activity Award 2019.

**Wang Peng** (F'18) received the B.Sc. degree in electronic engineering from Xian Jiaotong University, Xian, China, in 1978, the M.Sc. degree from Taiyuan University of Technology, Taiyuan, China, in 1987, and the M.Sc. and Ph.D. degrees in electrical engineering from the University of Saskatchewan, Saskatoon, SK, Canada, in 1995 and 1998, respectively. Currently, he is a full Professor with the School of Electrical and Electronic Engineering at Nanyang Technological University, Singapore. He is an Associate Editor or Guest Editor-in-Chief of *IEEE Transactions on Smart Grid*, *IEEE Transactions on Power Delivery*, *Journal of Modern Power Systems and Clean Energy*, *CSEE Journal of Power and Energy Systems*, and so on. His current research interests include power system planning and operation, renewable energy planning, solar/electricity conversion system and power system reliability analysis.